Title page

Characterizing subtypes of heart failure with preserved ejection fraction: the HeartMagic prospective observational study

Philippe Meyer[1], Angela Rocca[2], Jaume Banus[3], Augustin C. Ogier[3], Costa Georgantas [3], Pauline Calarnou [3], Anam Fatima[4], Jean-Paul Vallée[4], Jean-François Deux[4], Aurélien Thomas[5,6], Julien Marquis[7], Pierre Monney[2], Henri Lu[2], Jean-Baptiste Ledoux[3,8], Cloé Tillier[1], Lindsey A Crowe[4], Tamila Abdurashidova[2], Jonas Richiardi [3], Roger Hullin[2], Ruud B. van Heeswijk[3]

Corresponding authors: Ruud B. van Heeswijk (ruud.van-heeswijk@chuv.ch - primary), Philippe Meyer (philippe.meyer@hug.ch), Jonas Richiardi (Jonas.richiardi@chuv.ch), Roger Hullin (Roger.Hullin@chuv.ch)

1. Cardiology Division, University Hospital of Geneva, Geneva, Switzerland
2. Cardiology Division, Lausanne University Hospital (CHUV), Lausanne, Switzerland
3. Department of Radiology, Lausanne University Hospital (CHUV) and University of Lausanne (UNIL), Lausanne, Switzerland
4. Radiology Division, Diagnostic Department, Geneva University Hospitals and University of Geneva, Geneva, Switzerland
5. Faculty Unit of Toxicology, CURML, Faculty of Biology and Medicine, University of Lausanne, Lausanne, Switzerland
6. Unit of Forensic Toxicology and Chemistry, CURML, Lausanne and Geneva University Hospitals, Lausanne, Geneva, Switzerland
7. Lausanne Genomic Technologies Facility, University of Lausanne, Lausanne, Switzerland.

8. CIBM Center for Biomedical Imaging, Lausanne and Geneva, Switzerland

Abstract

Background

Heart failure (HF) is a life-threatening syndrome with significant morbidity and mortality. While evidence-based drug treatments have effectively reduced morbidity and mortality in HF with reduced ejection fraction (HFrEF), few therapies have been demonstrated to improve outcomes in HF with preserved ejection fraction (HFpEF). The multifaceted clinical presentation is one of the main reasons why the current understanding of HFpEF remains limited. This may be caused by the existence of several HFpEF disease subtypes that each need different treatments. There is therefore an unmet need for a holistic approach that combines comprehensive imaging with metabolomic, transcriptomic and genomic mapping to subtype HFpEF patients.

Methodology

This prospective multi-center observational cohort study will include 500 consecutive patients with actual or recent hospitalization for treatment of HF with preserved ejection fraction at two Swiss university hospitals, along with 50 age-matched HFrEF patients and 50 age-matched healthy controls. Diagnosis of heart failure is based on clinical signs and symptoms and subgrouping HF patients is based on the left-ventricular ejection fraction. In addition to routine clinical workup, participants undergo genomic, transcriptomic, and metabolomic analyses, while the anatomy, composition, and function of the heart are quantified by comprehensive echocardiography and magnetic resonance imaging (MRI). Quantitative MRI is also applied to characterize the kidney. The primary outcome is a composite of one-year cardiovascular mortality or rehospitalization. Machine learning (ML) based multi-modal clustering will be employed to identify distinct HFpEF subtypes in the holistic data. The clinical importance of these subtypes shall be evaluated based on their association with the primary outcome.

Discussion

The integration of comprehensive MRI with extensive genomic and metabolomic profiling in this study will result in an unprecedented panoramic view of HFpEF and should enable us to distinguish functional subgroups of HFpEF patients. This approach has the potential to provide unprecedented insights on HFpEF disease and should provide a basis for personalized therapies. Beyond this, identifying HFpEF subtypes with specific molecular and structural characteristics could lead to new targeted pharmacological interventions, with the potential to improve patient outcomes. Clinical trial number: not applicable.

Keywords

Heart failure, HFpEF, CMR, quantitative MRI, genomics, machine learning, metabolomics, subtyping, echocardiography

Background

Heart failure (HF) is a major public health concern, with a prevalence nearing 3% of the general population in most European countries that leads to substantial morbidity, mortality, and healthcare costs.[1] HF is classified into three categories based on left ventricular ejection fraction (LVEF): “HF with reduced ejection fraction” (HFrEF) when LVEF is ≤40%, “HF with mildly reduced ejection fraction” (HFmrEF) when LVEF is between 41% and 49%, and “HF with preserved ejection fraction” (HFpEF) when LVEF is ≥50% .[2,3] Over the past three decades, the proportion of patients with HFpEF has increased progressively with respect to patients with HFrEF, making HFpEF the predominant form of HF in Western countries, now accounting for over 50% of all HF cases.[1,4]

Many patients presenting with HF and an LVEF ≥50% exhibit specific cardiac conditions, such as infiltrative, hypertrophic, or restrictive cardiomyopathy, as well as valvular or pericardial diseases, which are now referred to as “HFpEF mimics”[5] or “secondary HFpEF”.[6] Therefore, a diagnosis of HFpEF should be considered only after excluding these mimicking or secondary conditions. With improved

diagnostic capabilities, recent evidence suggests that many of these patients may have been inadvertently included in earlier HFpEF studies.[7] Since elderly patients with HF and an LVEF ≥50% are often not comprehensively investigated, contemporary studies may still include these "false" HFpEF patients.

Even "primary" HFpEF is a heterogeneous syndrome.[6] The prevailing theory suggests LV diastolic dysfunction as the central pathomechanism, leading to abnormal hemodynamics with increased LV filling pressures and reduced cardiac output at rest or during exercise. In recent years, systemic microvascular endothelial inflammation resulting from hypertension, obesity, diabetes, chronic obstructive pulmonary disease, sedentary lifestyle, or iron deficiency has been the most widely accepted pathophysiological concept.[8–10] This systemic inflammation has been associated with myocardial inflammation and fibrosis as well as increased oxidative stress. In addition, systemic inflammation was related with activation or silencing of signaling pathways with subsequent cardiomyocyte remodeling and dysfunction.

However, the pathophysiology of HFpEF extends beyond more LV diastolic dysfunction, since LV systolic and left atrial function are also impaired. Furthermore, pulmonary vascular disease, right ventricular dysfunction, systemic arterial stiffening, coronary and peripheral microvascular dysfunction, chronotropic incompetence, skeletal muscle dysfunction, and arrhythmias (particularly atrial fibrillation) also contribute to HFpEF pathogenesis.[11,12]

Despite testing of multiple pharmacological compounds in large phase 3 clinical trials, many have failed to demonstrate treatment benefit within the specified period of observation.[13] Recently, sodium-glucose cotransporter-2 ($SGLT_2$) inhibitors and the non-steroidal mineralocorticoid receptor antagonist finerenone have demonstrated significant benefits in patients with HFmrEF and HFpEF.[14–16] However, although trials evaluating these therapies have shown reductions in composite morbidity and mortality endpoints, no single study has yet demonstrated a significant reduction in overall mortality or cardiovascular-related deaths in patients with HFpEF.[17] One potential explanation for the failure of

most trials targeting HFpEF is the heterogeneous pathophysiology of distinct HFpEF subtypes, which may each require a tailored therapeutic approach rather than a uniform "one size fits all" strategy.[6,18,19] Furthermore, the inclusion of HFpEF mimics in some studies may have confounded the results.[7] Finally, the relatively slow progression of HFpEF disease may require longer observational periods than those used in clinical trials.[18]

Numerous authors and major medical societies have recently made significant efforts to define distinct HFpEF phenotypes, aiming to identify specific subgroups that may benefit from targeted therapies. The Heart Failure Association (HFA) of the European Society of Cardiology (ESC) has developed an algorithm to better define a phenotype-based approach for HFpEF treatment.[6] This algorithm categorizes seven different clinical HFpEF phenotypes and proposes phenotype-specific treatment strategies for each. Examples of phenotype-specific treatments include semaglutide (a Glucagon-Like Peptide-1' (GLP-1) receptor agonist) and tirzepatide (a GLP-1 and glucose-dependent insulinotropic polypeptide (GIP) agonist), which have recently shown promise in treating the obese phenotype of HFpEF patients.[20–23] However, substantial overlap exists between these seven phenotypes, suggesting that this approach may not fully capture the complex heterogeneity of HFpEF disease.

New strategies that extend beyond routine clinical data are therefore necessary. The present study pursues an integrative multi-modal approach to generate a highly comprehensive dataset on HFpEF using advanced modalities that delve deeply into anatomy, genetics, and metabolism. The approach will leverage cutting-edge technologies not yet available in routine clinical practice.[13] Magnetic resonance imaging (MRI) is particularly well-suited for the anatomical and functional components, as it allows for precise quantification of cardiac structure, function, hemodynamics, and tissue composition at high resolution.[24] When combined with genomic and metabolomic data, such rich imaging information provides an ideal foundation for applying statistical models trained using machine learning (ML). ML has recently revolutionized various healthcare fields by enabling the analysis of complex, high-dimensional data to uncover patterns, make accurate predictions, and support decision-making with unprecedented speed and precision.[25] Applying ML-based techniques to the

abovementioned comprehensive dataset of HFpEF disease is thus timely, and has the potential to drive breakthroughs in our understanding of HFpEF pathophysiology.

In summary, in this observational study named HEARTMAGIC (HEART failure studied with a MAchine learning, Genomics, and Imaging Combination), we aim to conduct an unbiased and comprehensive subtyping of HFpEF patients, focusing on the underlying pathophysiology in relation to specific clinical outcomes (Central Figure). This approach holds groundbreaking potential for identifying precise therapeutic targets. To achieve this, we will establish the largest HFpEF databank to date, integrating clinical, genomic, metabolomic, and quantitative MRI data.

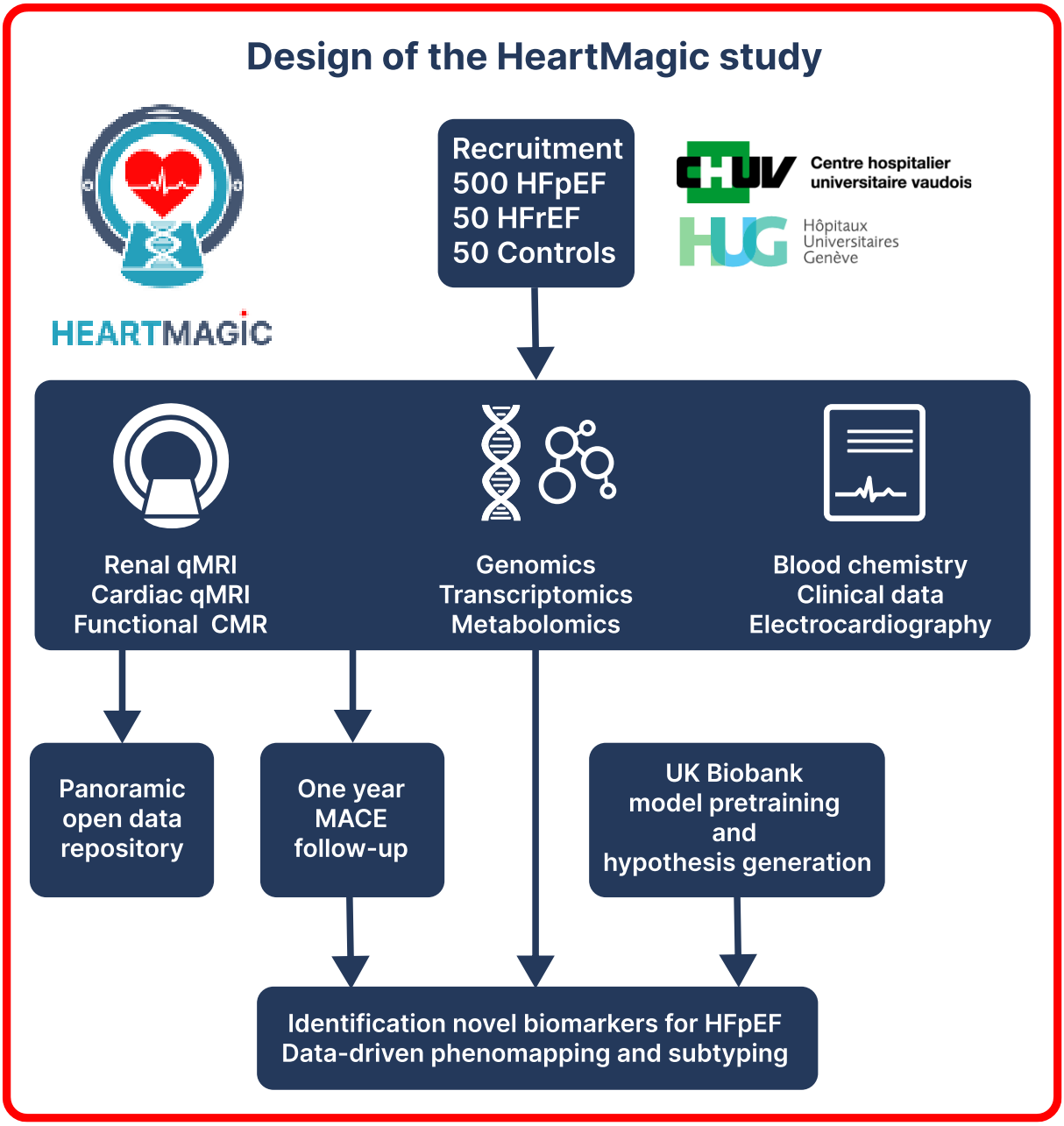

Central Figure. *Setup and design of the HeartMagic study.*

Design and Methods

Aim and Study Design

The goal of this project is to establish a comprehensive database of individual HFpEF patient data to characterize HFpEF disease in-depth and to identify clinically relevant subtypes with actionable

therapeutic targets. To this end, we will collect multi-modal MRI and echocardiography of the thorax and kidneys together with clinical, genomic, transcriptomic, and metabolomic data. Clinical trial numbers were not obtained from any registry since this is an observational study and not a clinical trial.

This prospective observational clinical study does not interfere with standard care, and no randomization is required. A total of 500 consecutive patients with current or recent hospitalization for acute heart failure and preserved LVEF at the Geneva University Hospitals (HUG) or the Lausanne University Hospital (CHUV) will be enrolled, along with 50 HF patients with reduced LVEF and 50 age-matched healthy controls. Recruitment is planned over a 3-year period based on acute HF hospitalization rates at both centers. Each participant will undergo genetic, genomic, and metabolomic analyses, comprehensive echocardiography, and quantitative MRI. HF patients will receive a follow-up by phone at 30, 90 days and one year post-discharge.

Setting

The study is conducted at two Swiss academic centers: the Geneva University Hospitals (HUG) and the Lausanne University Hospital (CHUV). HUG has approximately 2,000 beds, while CHUV has roughly 1,500 beds. Both are tertiary care facilities that serve a population of over 2 million people across their respective regions. Each year, approximately 1,200 patients are hospitalized for acute heart failure at HUG, while CHUV admits around 700 patients for the same condition according to the Swiss Federal Office of Statistics.

Patients

The study will prospectively include 500 HFpEF patients, while simultaneously recruiting 50 HFrEF patients and 50 healthy participants, age- and sex-matched to the HFpEF group (Table 1). The latter two groups will serve as control groups.

***Table 1**. The expected distribution of recruitment across the two sites.*

	CHUV	HUG	Total
HFpEF patients	290	210	500
HFrEF patients	30	20	50
"Healthy" volunteers	30	20	50
	350	250	600

For patients with HFpEF the inclusion criteria are:

1. Adult ≥18 years old
2. Written and informed consent
3. Presence of dyspnea
4. Current or recent hospitalization for acute HF treatment with signs of pulmonary and/or systemic congestion
5. Left ventricular ejection fraction (LVEF) ≥50% on echocardiography with at least 1 structural and/or functional cardiac abnormality compatible with HFpEF according to the current HFpEF definition.[3,26]

The exclusion criteria are:

1. Claustrophobia, ferromagnetic implants, or any other contra-indications to MRI
2. Contraindication to adenosine/regadenoson and/or gadolinium-based contrast agents
3. Pregnant or breastfeeding women
4. Other causes of HF amenable to specific treatment (coronary artery disease, >moderate valvular dysfunction, active endocarditis), sleep apnea, alcohol abuse with >15 g alcohol/day, symptomatic

hyper- or hypothyroidism, >mild anemia, >moderate chronic obstructive bronchopulmonary disease, pneumonia

5. Cardiac amyloidosis or other infiltrative cardiac disease
6. Comorbid conditions associated with life expectancy <1year
7. Systemic inflammatory disease of rheumatic or immunological origin
8. Incapacity of judgement
9. Active Covid-19 infection
10. Unwillingness to receive notice of accidental findings
11. A body size prohibitive for the 60cm-diameter bore of the MR scanner

HFrEF patients are age- and gender-matched with HFpEF patients and share similar inclusion criteria, except for an LVEF <40%, as well as comparable exclusion criteria. Healthy volunteers (aged ≥60 years) must have NT-proBNP levels at or below the age-adjusted upper limit and no history of cardiac disease or more than moderate hepatic disease. They are also age- and gender-matched with the HFpEF group and share similar exclusion criteria with the other two groups.

Recruitment

Patients hospitalized for dyspnea at the emergency department (ED) are screened for the presence of preceding acute decompensated heart failure in the last 12 months. The presence of symptoms of heart failure, etiology of heart failure, past medical history, initial blood chemistry, echocardiographic evaluation of left ventricular ejection fraction, presence of cardiovascular devices and other ferromagnetic materials are assessed. Patients who meet the inclusion criteria are approached after their referral to the internal medicine and cardiology wards, given a consent form, and have 48 hours to make a decision. The scheduled enrolment of 500 HFpEF patients, 50 HFrEF patients, and 50 healthy controls is expected to be complete by the end of 2026. Weekly surveillance of the age and sex of recruited patients is used to assure a balanced study population. The female-to-male ratio will align with the sex prevalence in the general population at 2:1 for HFpEF and 1:4 for HFrEF patients.

Age-matched healthy controls are recruited via the University for Seniors in Lausanne and Geneva through online advertisement. Interested individuals attend an information session, complete the informed consent process, and are compensated with CHF 200.

Patient Study Procedure

Each patient is invited to remain in follow-up for up to 1 year after inclusion, which aims to document routine care. The study procedures are divided into three parts (Figure 1):

1. Enrollment and Information visit: the patient receives information about the study's purpose, procedures, risks, and benefits. After reviewing and discussing the informed consent form (ICF), the patient has the opportunity to ask questions before deciding to participate. If the patient agrees, they sign the ICF, and the next steps are arranged.
2. Baseline visit (Day 1): blood (~40 mL) are collected. Transthoracic echocardiography and cardiac MRI are also performed on the same day.
3. Follow-up at Days 30, 90, and 365: Follow-up is by phone and documents patient-related outcomes (morbidity, mortality, healthy changes), which are validated through medical documentation in a second step. If a health issue has arisen, the participant is invited for an additional ambulatory visit at CHUV/HUG.

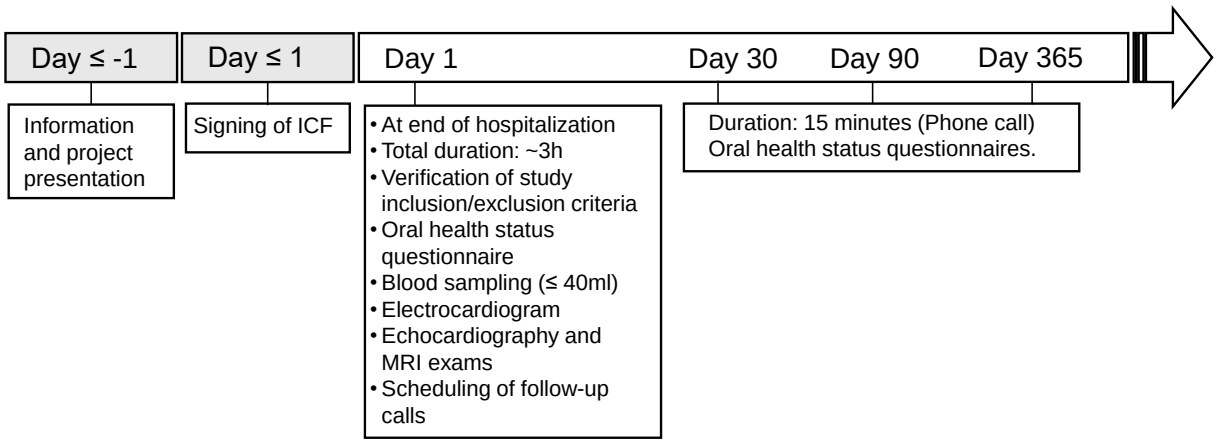

Figure 1. *Flow chart of the study procedure.*

Blood sampling

Blood samples are used for the analysis of metabolomics, genomics, transcriptomics, and clinical chemistry. After cubital venipuncture, tubes for each of these analyses are filled with blood. Blood for analysis of clinical chemistry and the hemogram are analyzed by the local Departments of Laboratory Medicine (Supplementary Table 1); samples for other measures are aliquoted, frozen and stored at -80°C, and sent abroad in batches of 96 samples. The assessment of blood parameter associated with systemic inflammation uses the human proinflammatory panel I (MESO SCALE DISCOVERY®) cytokine assay (K15052D), which measures interferon γ (IFNγ), interleukin-1ß (IL-1ß), interleukin-6 (IL-6), interleukin-10 (IL-10), and tumor necrosis factor α (TNFα).[27]

Metabolomics

2.5 mL of whole blood is withdrawn in lithium heparin tubes and centrifuged to obtain plasma. Plasma is aliquoted in tubes that allow the storage of samples at -80°C and sent in batches of 96 to the University Center for Legal Medicine of Lausanne and Geneva for analysis (CURML). There, metabolites are extracted from 100 µL of plasma using a cold methanol-ethanol-water solvent mixture in a 2:2:1 ratio. Samples are analyzed in full scan mode in both positive and negative polarities using an ultra-high performance liquid chromatography system coupled with a Thermo Scientific high-resolution xploris 120 mass spectrometer (HRMS) in RP (Kinetex C18, in positive and negative modes). Separation is performed in gradient elution mode with mobile phases in positive mode (H2O ; 0.1% formic acid and MeOH; 0.1% formic acid) and in negative mode (H2O ; 5mM Ammonium acetate + 0.25mM Ammonium fluoride and MeOH) This will allow detection of several thousand metabolite features, as described previously.[28,29] The expected overlap of compounds between the different approaches is used as an internal validation to assess the adequacy of our results. Raw UPLC-HRMS are processed using Compound Discover 3.3 software for peak detection, chromatogram alignment, and isotope annotation. To provide the highest quality data for bioinformatics mining, quality controls (i.e., representative pool of samples) and internal standards are used to assess overtime-analytical drift (i.e., batch effects).[30] To tackle this issue, we will use a method called systematic error removal using

random forest (SERRF) and "DBnorm", which includes algorithms for preprocessing and removing technical heterogeneity from the data via a statistical model in a two-stage procedure.[31] The determination of the metabolomic signature has the potential to highlight discriminant metabolites significantly different between subtypes of the HFpEF umbrella.

Over the last few years, several large-scale metabolomics studies on thousands of biological samples have been performed on the platform described above.[32,33] The human metabolome has not been completely covered, nonetheless, the discriminant metabolites will be characterized using both their MSn fragmentation pattern and open-access libraries.[34] With accurate mass measurement, a home-made script will first be used to identify discriminant metabolites according to a predefined m/z list of metabolites. This list, including around five thousand present and/or detected metabolites in biofluids, is built from the human metabolome database (HMDB) and updated from our own library. We additionally use the human metabolome database (www.hmdb.ca), lipidmaps (www.lipidmaps.org), metlin (http://metlin.scripps.edu/index.php), and mzcloud (www.mzcloud.org), together including more than 40,000 entries. Identification will also b then performed using SIRIUS 4.7.4, a software that determines the most likely elemental composition of metabolites through the analysis of isotopic patterns and MS/MS fragmentation spectra, and CANOPUS, a computational tool for systematic annotation of compound chemical classes.[35,36]

Genomics

1.2 mL of whole blood is withdrawn in EDTA-K3E tubes and then aliquoted in tubes that allow the storage of samples at -80°C and sent in batches of 96 to INRAE (the French National Research Institute for Agriculture, Food, and Environment, based in Paris, France) for DNA extraction and genotyping in batches of 96 samples, including a mix of controls, HFpEF, and HFrEF patients. Genotyping is performed on the GENTYANE INRAE Clermont platform (UMR GDEC n°1095 INRAE/UCA, https://gentyane.clermont.inrae.fr/) using the Axiom Precision Medicine Diversity Array (PMDA) (Thermo Fisher Scientific, Waltham, MA, USA), which provides over 93% marker overlap with the UK

Biobank Axiom array in the categories of interest for polygenic risk scores (see below), and over 800K markers in the imputation grid, ensuring that we can match with UKB genomic data. Data are provided in CEL format.

Transcriptomics

For gene expression, 2.5 mL of whole blood is stored in PAXgene tubes at -80°C, and sent to QiaGen (Hilden, Germany) on dry ice for RNA extraction. Sequencing is performed at the Lausanne Genomic Technologies Facility, University of Lausanne, Switzerland (https://www.unil.ch/gtf). Sequencing libraries are prepared from 500 ng total RNA using the Illumina Stranded mRNA kit from Illumina. Globin depletion is performed using the FastSelect kit from Qiagen. Sequencing is performed on an Aviti sequencer (Element Biosciences, San Diego, CA, USA) using single-end sequencing with 150 cycles, at a coverage of 25M reads per sample. Sequencing data is demultiplexed using the Bases2Fastq 2.0 software, quality checked using Fastqc v0.11.9 (https://www.bioinformatics.babraham.ac.uk/projects/fastqc/) and Fastq Screen,[37] and finally provided in FASTQ format.

Electrocardiography

Patient electrocardiograms (ECGs) are read manually by a cardiologist and trained electrophysiologist and also automatically by applying the BRAVO and GLASGOW algorithms.[38–40] In case of > 25% difference between measures of a single parameter between the manual and the automated reading of the same ECG, the difference is discussed between the manual operator and another expert of ECG reading.

Transthoracic Echocardiography

TTE is routinely performed once patients are euvolemic and comfortable in the supine position. All examinations are conducted on an Epiq CVx-3D Ultrasound system (Philips Healthcare, Eindhoven, the Netherlands) using an X5-1c 3-dimensional transthoracic probe. A comprehensive 2-dimensional

examination is performed initially.[41] Additionally, 3-dimensional acquisitions of the left ventricle and left atrium are obtained using the Dynamic Heart Model automated 3D tool (Philips Healthcare, Eindhoven, the Netherlands), and 3D images of the right ventricle are captured using the 3D-autoRV tool (Philips Healthcare, Eindhoven, the Netherlands). Longitudinal strain of the left ventricle, left atrium, and right ventricular free wall are assessed using the Autostrain LV, Autostrain LA, and Autostrain RV postprocessing tools, respectively (Philips Healthcare, Eindhoven, the Netherlands). All measurements adhere to the recommendations from the European Association of Cardiovascular Imaging for chamber quantification,[42] evaluation of left ventricular diastolic function,[43] and the European consensus on the diagnosis and imaging of HFpEF.[26,44] Valvular disease is classified as mild, moderate, or severe according to current guidelines.[45–47] The list of echocardiographic measurements is presented in Supplementary Table 1.

Magnetic Resonance Imaging

Image Acquisition

Study participants are scheduled for a one-hour MRI exam on a fully CE-marked clinical 3 tesla (T) scanner (Prisma or PrismaFit, Siemens Healthineers, Erlangen, Germany) of the Center for BioMedical Imaging (CIBM) located in the Departments of Radiology of the CHUV and the HUG. Scanning is always performed by a technologist trained for cardiac research scans or a radiologist specialized in cardiac MRI, and a cardiologist is present for the injection of the pharmacological stressor. Besides routine localizer scans, this one-hour exam subsequently consists of (**Table 2**):

1. Kidney morphology: Coronal and transverse T_2 HASTE.
2. Kidney oxygenation: Breath-held coronal BOLD T_2* mapping.
3. Kidney tissue characterization: free-breathing coronal native joint T_1-T_2 mapping (PARMA – PARametric MApping) to quantify interstitial fibrosis and edema.
4. Cardiac function: routine 2D cine of the heart (short-axis stack, two-chamber, three-chamber, four-chamber, and left-ventricular outflow tract views).

5. Cardiac flow: 2D flow just above the level of the aortic valve to measure the ejected blood volume.
6. Myocardial tissue characterization: free-breathing 2D native joint T_1-T_2 mapping (PARMA) to quantify interstitial fibrosis and edema at the basal, mid-ventricular, and apical short-axis as well as the four-chamber orientations.
7. Stress myocardial perfusion: if eGFR>30mL/min/1.73m^2, quantitative myocardial perfusion imaging (qPerf) after the injection of a pharmacological stressor (100 mg adenosine or 400 µg regadenoson) Either stressor is applied since they are part of the local protocols; in addition, their effect on the physiologically in equivalent.[48] This is followed by a half-dose of gadolinium-based contrast agent (GBCA; 0.05 mmol/kg gadobutrol (Gadovist, Bayer AG) or 0.1 mmol/kg gadoteric acid (Dotarem, Guerbet)) during the acquisition.
8. Cardiac anatomy and function: A second half-dose of GBCA is immediately followed by free-running 5D imaging (5D FRF) to assess anatomy and function at isotropic high spatial resolution in addition to the routine 2D cine.
9. Thoracic flow: 4D (i.e. 3 spatial dimensions over time) flow imaging to quantify the flow patterns and velocities in the heart and great vessels.
10. Post-contrast myocardial tissue characterization: repetition of the free-breathing joint T_1-T_2 mapping 8-18min after the injection of the second dose of GBCA, now to quantify the extracellular volume (ECV).
11. Quantitative myocardial rest perfusion imaging: the same scan as the stress perfusion imaging, without the stressor and with a third half-dose of GBCA.

After the scan, images and raw k-space data are directly saved to secured servers managed by the CHUV and HUG information technology departments.

Late gadolinium enhancement (LGE) imaging for the visualization of myocardial scar tissue is not performed because it has been demonstrated that *small* focal scars do not affect the outcome of HFpEF,[49] while larger scars are visualized on the post-GBCA T_1 maps, ECV maps, and synthetic LGE maps.[50]

1

2 ***Table 2.*** *MRI pulse sequence parameters.*

Sequence	HASTE	BOLD	PARMA	2D cine	qPerf	5D FRF	4D flow
Sequence type	TSE	ME-GRE	GRE	bSSFP	GRE	GRE	GRE
Dimensions	2D	2D	2D	2D	2D	5D	4D
TE (ms)	96	6-52	1.5	1.28	0.98	1.33	2.25
TR (ms)	1600	76	3.36	3.39	1.99	2.99	4.27
Echoes	205	12	1	1	1	1	1
Flip angle (°)	80	30	12	43	14	15	12
Matrix size	256x256	256x256	192x192	256x170	192x114	160x160x 160	160x102x 39
Field of view (mm^2)	280x280	400x400	300x300	380x285	360x270	220x220x 220	380x304x 120
Slices	10	1	1	1-12	3	-	-
Slice thickness (mm)	5	5	8	8	8	1.38	2.5
Acceleration	GRAPPA, PF	-	CS	CS	GRAPPA, PF	CS	GRAPPA/ CS
ECG triggering	N	N	Y	Y	Y	N	Y
Resp MoCo	BH	BH	LL-NAV	BH	FB	SN	LL-NAV

Temp resolution (ms)	-	-	151	HB/25	227ms	HB/25	HB/25
k-Space trajectory	Cart	Cart	GA-Rad	Cart	Cart	GA-Rad	Cart
Inline recon	Y	Y	N	Y	Y	N	Y
Acquisition duration	16s	23s	25-40HB	2-24s	90HB	4m05s	4m37s-9m
Prep module(s)	-		T_2p, IR	-	Sat	-	-
Reference	[51]	[52]	[53]	[54]	[55]	[24]	[56]

* ME-GRE multi-echo GRE, bSSFP balanced steady-state free precession, BH breath hold, GA golden angle, FB free breathing, HR heart rate, HB heartbeat, Cart Cartesian, Rad radial, IR inversion recovery, T_2p T_2 preparation, GRAPPA GeneRalized Autocalibrating Partial Parallel Acquisition, PF partial Fourier, CS compressed sensing

Image and Map Reconstruction

HASTE images and BOLD maps of the kidney as well as 2D cine, qPerf, and 4D flow of the heart are reconstructed on the scanner with manufacturer software. Raw data of the PARMA and 5D FRF acquisitions are exported to a separate workstation for image and map reconstruction.

For the PARMA joint T_1-T_2 maps of both the kidney and heart, source images are reconstructed with compressed sensing.[53] The extended phase graph formalism is employed to simulate a dictionary of signals for a broad range of T_1 and T_2 values. This dictionary is acquisition-specific and must be generated for each scan, as heart rate and respiratory gating influence magnetization evolution. The reconstructed images are matched pixel-by-pixel to the closest dictionary entry using a dot product, resulting in T_1 and T_2 maps.

For the free-running 5D images, cardiac and respiratory motion signals are self-gated and extracted from the raw data using the repeated superior–inferior (SI) projections of the 3D radial trajectory.[57] Principal component analysis is first applied to separate the respiratory components, and second-order blind identification is used to isolate the cardiac components.[58] A Gaussian fit is applied to the power spectral density of each resulting component to identify the cardiac signals,[59] which favors the extraction of signals with a fundamental frequency within the expected physiological range. These physiological signals are subsequently used to bin the acquired data into cardiac and respiratory phases as previously described,[24] resulting in undersampled 5D data. Respiratory binning is achieved by dividing the respiratory signal into four equally populated phases, ranging from end-expiration to end-inspiration. The cardiac signal is used to organize the data into non-overlapping phases of 50 ms. Finally, a k-t sparse SENSE compressed sensing algorithm is employed to reconstruct the 5D whole-heart images.[24,60] Cardiac and respiratory regularization weights are set to 0.005 and 0.03, respectively, to ensure optimal reconstruction quality while maintaining the temporal and respiratory coherence of the data.

Clinical Data

We collect data related to hospitalization duration (timings), movements between the services, interventions, medication, and imaging exams from the hospital information systems (Supplementary Table 4). All patient-related clinical data are coded. Participant data from both hospitals are collected in an eCRF. The database used for data storage in this study is RedCap®. The database is located on a secure institutional server at the CHUV, with protected access.

Data Analysis and Statistics

Overall strategy

The statistical analysis plan focuses on developing imaging and genomics analysis methods applicable to the UK Biobank (UKB), which is our discovery cohort, and applying these methods on our own data

to validate our findings. While UKB is a community sample and not clinically enriched in HFpEF patients, its large size makes it suitable as a development and discovery dataset around heart failure, cardiovascular disease more generally, and HFpEF risk factors. Using the validated H2FPEF risk score as a surrogate for HFpEF diagnosis[61] will be considered, although it is limited by several factors: 1) trans-thoracic echocardiography is not available in UKB, leading to a truncated maximum score. 2) the score is meant to be applied to patients presenting with dyspnea, rather than a generic population. Diagnostic uncertainty is further increased by lack of NT-proBNP values for UKB subjects.

Initially, we will use group comparisons to identify differences in each of the modalities between the different clinical groups available in our dataset, as well as unsupervised methods within the HFpEF group. In a second step, we will resort to survival analysis (time-to-event analysis for the primary outcomes of the study), in particular within the HFpEF group, to focus on clinically relevant disease subtypes. Finally, we will focus on integrative analysis, where multiple modalities (clinical, imaging, ECG, genomics, transcriptomics, metabolomics…) are considered jointly for subtyping.

MR Image and Map Analysis

Renal diameters and volume, medullary and cortical thickness and volume are derived from the HASTE series. In the renal T_1, T_2, and T_2* maps the cortex and medulla are automatically segmented with a deep-learning-based 2D U-Net.[62]

In the routine 2D cine images, LV and RV blood and myocardial volumes and mass, LVEF, RVEF, LA and RA volumes are manually segmented. The results in the first 100 subjects are then used to train DL-based automated segmentation networks for the 2D cines. LV long-axis systolic function is measured using mitral annular systolic excursion and LV global longitudinal strain (GLS). Left and right total atrial emptying fraction, passive atrial emptying fraction and active atrial emptying fraction are measured from the maximum LA and RA volumes, the prior to atria contraction and the minimum atrial volumes as reported by Kowallick et al.[63]

We also use these 2D cine data to develop methods to study spatio-temporal patterns. We process the images, segment the ventricles and divide the myocardium in different regions (16 AHA sub-segments for the left ventricle myocardium, 9 segments for the right ventricle myocardium). These divisions give us the flexibility to represent the heart as a spatio-temporal graph in which the nodes represent these myocardium regions and edges represent similarities between segments. Used across multiple acquisition sequences (relaxometry, strain, motion, etc.), these structural heart graphs will represent quantitative tissue properties, mechanical properties, and structural properties of the heart using a unified representation. The goal is to identify key functional and anatomical properties that are relevant to quantify the cardiac function and the cardiovascular health. The use of graph neural networks will allow the use of low-dimensional, latent representations of structure and function.

Similarly, from the 5D FRF images[24] we extract global measures such as the diastolic and systolic atrial and ventricular volumes, as well as segmental myocardial measures such as wall thickness and strain. To assess the presence of pulmonary hypertension for the H2FPEF composite score,[61] we calculate the septal-to-free-wall curvature ratio.[64]

Myocardial T_1 and T_2 values are manually segmented on the PARMA maps according to the standardized 17 AHA LV segments,[65] as well as for their equivalent RV segments where available.[66]

Subendocardial and subepicardial as well transmural myocardial perfusion is quantified in 16 sectors at 3 level (basal, mid and apical) according to the Kellman method.[67]

In the 4D flow MRI we measure aortic and pulmonary flow, flow through the atrioventricular and ventriculo-arterial valves, the transmitral flow profile, wall shear stress (WSS) at the level of the aorta and pulmonary artery, and pulse wave velocity (PWV) in the aorta. An analysis of the components of intraventricular flow and turbulence in the left atrium are performed on a dedicated software (Cvi 42, Circle, Montreal, Canada). Peak early diastolic tissue velocity (e') is assessed at the septal and lateral mitral annulus using automated mitral valve tracking. Mitral inflow velocities (E and A) are measured and combined with e' to measure the average septal-lateral E/e' ratio reflecting pulmonary capillary

wedge pressure. Tricuspid annular plane systolic excursion (TAPSE) and peak tricuspid annular systolic tissue velocity (S') is measured as indices of right ventricular (RV) longitudinal systolic function.

To identify associations between the image-based biomarkers and clinical outcomes we will further develop systematic screening approaches with careful propensity matching and survival analysis[68] to relate these potential biomarkers to clinical outcomes.

Omics preprocessing and analysis

For genomic data, we will apply standard quality control (QC) and preprocessing[69] including sample quality checks (sex inconsistencies, call rate…), marker quality checks (minor allele frequency, Hardy-Weinberg equilibrium), and batch effect analysis and correction, using the bigsnpr package[70] and other in-house tools.

For metabolomic data, after acquisition, preprocessing and QC steps described above, we will use the negative and positive mode results separately (around 8000 metabolites in total), obtained from untargeted analysis, to narrow down the list to around 200 metabolites for in-depth characterization. This will be done by clinical group comparison, as well as correlation screening with respect to imaging features of interest, survival-linked features of interest, and associations with selected genes and SNPs.

For transcriptomic data, we will run an established QC pipeline (RNA-SeQC2[71]), annotate to the latest genome assembly, and quantify gene expression using Salmon[72] (using the alternative pipeline of first aligning with STAR[73] and quantifying using HTSeq)[74].

Novel biomarkers for HFpEF

The main focus will be to find biomarkers with outcomes-linked differences within the HFpEF group, in particular using survival analysis ("survival subtypes"). Because the follow-up period is one year and the recruitment is ongoing, during the time period where event counts are insufficient for modelling, we will in the initial analysis phase focus instead on unsupervised subtyping ("phenotyping subtypes") and supervised group characterization. Then, when outcomes are observed, clustering results will be

evaluated by looking at the silhouette coefficient, the concordance index, normalized mutual information (NMI), and the adjusted Rand index (ARI) with respect to observed primary and secondary clinical outcomes.

Another approach to mitigate the lack of events is to rely on the UK Biobank (UKB), a large observational cohort, for hypothesis generation. We use the UKB dataset to identify various CMR-derived biomarkers that have prognostic value on the risk of hospitalization and death due to heart failure, as well as other co-morbidities associated with HFpEF.

A focus of the work is imaging genetics– using CMR-derived imaging phenotype as complex traits and GWAS targets. Preprocessed genomics data will thus be used for GWAS analyses (plink tool), in UKB for discovery, and our sample for validation. While cine and T_1 acquisitions are not the same in both datasets, the approach should allow us to narrow down the set of plausible candidates. From these, we will also generate low-dimensional representations of genomic data, to be included in subtyping analyses, by using our newly proposed transformer-based non-linear method for polygenic risk scoring.[75]

Throughout, we will use a combination of the omics available to obtain a better understanding of group differences, phenotyping subtypes, and survival subtypes. For example, we will look at consensus across omics, and look at e.g. differential gene expression between subtypes obtained from other omics and modalities, although this approach can struggle to exploit discordant relationships[76]. We will also pursue graph-based approaches, viewing the problem as a community detection problem on a multilayer graph.

These analyses aim to produce novel interpretable, predictive and reproducible biomarkers that can improve clinical decision making, refine prognostic estimates, and can be used to propose novel treatment avenues and secondary endpoints for future clinical trials.

Open access and open data

All studies and sub-studies will be published in an open access format. All data will be converted to depersonalised non-proprietary formats and will be deposited in FAIR online repositories for open access, except for genomic data, which will be deposited with access control.

Identifying attributes including names and dates of birth will be removed from all data. Then, data will be depersonalized according to its type: tabular data (clinical, blood chemistry, ECG features) will be depersonalized using tools such as ARX;[77] imaging data will be converted to Nifti before sharing, with potentially sensitive headers removed; sequence reads in transcriptomic data will be sanitized;[78,79] metabolomic data will be shared as is since is not thought to contain directly identifying information.

Discussion

This study protocol addresses the complex and heterogeneous nature of HFpEF, a prevalent condition with poor prognosis and no effective pharmacological treatments. By integrating advanced MRI with metabolomic, transcriptomic, and genomic analyses, this prospective observational study aims to refine HFpEF subtyping through machine learning (ML)-based multimodal clustering. With a cohort of 500 HFpEF patients, 50 age-matched HFrEF patients, and 50 healthy controls, we seek to identify clinically meaningful subgroups linked to distinct pathophysiological mechanisms and clinical outcomes, with a primary composite endpoint of one-year cardiovascular mortality or rehospitalization.

ML is central to precision medicine, particularly when applied to rich panoramic data such as genetics, metabolomics, proteomics, and quantitative MRI.[76] This study focuses on two ML strategies: integrative representations,[80] which merge omics and imaging data for improved disease characterization, and multimodal subtyping, which enhances phenotypic resolution. Graph-based representations, known for their interpretability and expressiveness, will play a key role in advancing core ML methodologies. Notably, network analysis has been described as a “grand unifier” in biomedical data science, underscoring its potential in HFpEF research.[81]

Identifying clinically relevant HFpEF subtypes remains a challenge, as prior subgroup analyses based on conventional parameters have yet to yield effective therapeutic targets. Evidence from cancer research suggests that integrating multiple biological measurements before subtyping can yield more consistent and clinically actionable classifications.[82] By applying this principle to HFpEF, we aim to overcome previous limitations and improve phenotyping strategies.

The inclusion of a large, well-characterized cohort, along with comparative groups of HFrEF patients and healthy controls, strengthens the study's generalizability and analytical depth. Furthermore, its prospective design and clinically relevant primary outcome measure ensure robust validation of the identified HFpEF subtypes, with the ultimate goal of advancing personalized treatment strategies.

Beyond the HFpEF pathology, it is expected that the integrative methods developed during this project will translate to other cardiovascular diseases and will also be relevant to several MRI radiogenomics studies such as hepatocellular carcinoma.

Feasibility

Description of team expertise, recruitment feasibility

The study protocol for this HFpEF project is highly feasible, supported by the multidisciplinary expertise of four main investigators and project partners, each contributing complementary skills to manage the protocol's complexity. Ruud van Heeswijk leads a radiology-embedded engineering team at CHUV, ensuring access to advanced MRI technology, secure data storage, and computational resources. Jonas Richiardi heads the translational machine learning lab, specializing in medical imaging techniques. Roger Hullin and Philippe Meyer lead the Heart Failure Units at CHUV and HUG, respectively, overseeing nearly 1,000 HFpEF patient cases each year. Each investigator directs one of three Work Packages: van Heeswijk (MRI), Richiardi (machine learning), and Hullin and Meyer (clinical study). Defined roles and collaborative structures across teams ensure effective data handling, patient recruitment, and ethical compliance, with research nurses in Hullin's and Meyer's units managing recruitment and follow-up. In addition, project partners provide required expertise, for example in

statistical genetics (Zoltan Kutalik and team), metabolomics (Aurélien Thomas and team), transcriptomics (Julien Marquis and team), advanced cardiac MRI (Matthias Stuber and team), clinical thoracic and abdominal imaging (Jean-Paul Vallée and team), and 4D flow (Jean-François Deux). Supported by CHUV's Clinical Trial Unit, this well-coordinated approach enables the team to address the complexities of HFpEF phenotyping.

Strengths and Limitation

As an observational study, our work is limited by its inability to establish causal relationships between identified HFpEF subtypes and outcomes. Additionally, for resource and logistical reasons, follow-up is limited to a year and potential medium- and longer- term outcomes will not be observed.

Our inclusion and exclusion criteria may limit the representativity of the sample, in particular with respect to comorbidities, which may be more prevalent in the general HFpEF population than in our sample. Likewise, while the study is already multi-centric, its focus on western Switzerland limits the representativity of our sample on a wider geographical scale.

The reliance on advanced imaging and molecular techniques may limit reproducibility in settings without similar resources, and the complexity of data analysis may pose challenges for real-time clinical application.

Despite these limitations, the study's extensive dataset could serve as a foundational resource for future HFpEF research, with potential to guide targeted therapeutic developments.

List of abbreviations

CE – Conformité européenne

CHUV – Centre Hospitalier Universitaire Vaudois (Lausanne University Hospital)

CMR – Cardiovascular Magnetic Resonance

eCRF – Electronic Case Report Form

EF – Ejection Fraction

HEARTMAGIC – HEART failure studied with a MAchine learning, Genomics, and Imaging Combination

HFpEF – Heart Failure with Preserved Ejection Fraction

HFrEF – Heart Failure with Reduced Ejection Fraction

HUG – Hôpitaux Universitaires de Genève (Geneva University Hospitals)

ICF – Informed Consent Form

LV – Left Ventricle

ML – Machine Learning

NT-proBNP – N-terminal pro–B-type Natriuretic Peptide

PARMA – PARametric MApping

qMRI – Quantitative Magnetic Resonance Imaging

qPerf – Quantitative Perfusion

RV – Right Ventricle

UKB – UK Biobank

Declarations

Ethics approval and consent to participate

Ethics approval was obtained from the Ethics Committee of the Canton of Vaud (CER-VD) of Switzerland under number 2022-00934. All participants provide written informed consent to participate prior to enrollment.

Consent for publication

All authors consent to this publication.

Availability of data and materials

It is planned to make all data available in a public repository after anonymization; this is detailed in the informed consent forms that all participants signed.

Competing interests

There are no competing interests.

Funding

The majority of the HeartMagic study is funded by the Swiss National Science Foundation (SNSF) under grant number CRSII5_202276.

Authors' contributions

Meyer, Richiardi, Hullin, and van Heeswijk wrote the initial draft of the manuscript. All authors significantly revised the manuscript. Van Heeswijk coordinates the study. Meyer and Tillier set up the recruitment and screening in Geneva; Hullin, Richiardi, Rocca, and Abdurashidova set up the recruitment and screening in Lausanne. Rocca set up the coordination between the project partner teams. Rocca, Tilier and Hullin set up the blood sampling and storage. Thomas established the metabolomic analysis. Marquis, Hullin, and Richiardi set up the genotyping and transcriptomics protocol. Hullin established the ECG analysis. Meyer and Monney set up the echocardiography protocol. Van Heeswijk, Ledoux, Vallée, Ogier, Crowe, Calarnou, Fatima, and Deux set up the MRI acquisition, reconstruction, and analysis. Rocca, Tillier, Meyer, and Hullin collected the clinical data. Richiardi, Banus, and Georgantas established the multi-modal data integration and analysis procedure.

Acknowledgements

This research is conducted using the UK Biobank Resource under Application Number 80108.

Authors' information (optional)

N/A

References

1. Savarese, G. *et al.* Global burden of heart failure: a comprehensive and updated review of epidemiology. *Cardiovasc. Res.* **118**, 3272–3287 (2022).
2. McDonagh, T. A. *et al.* 2021 ESC Guidelines for the diagnosis and treatment of acute and chronic heart failure. *Eur. Heart J.* **42**, 3599–3726 (2021).
3. Bozkurt, B. *et al.* Universal definition and classification of heart failure: a report of the Heart Failure Society of America, Heart Failure Association of the European Society of Cardiology, Japanese Heart Failure Society and Writing Committee of the Universal Definition of Heart Failure: Endorsed by the Canadian Heart Failure Society, Heart Failure Association of India, Cardiac Society of Australia and New Zealand, and Chinese Heart Failure Association. *Eur. J. Heart Fail.* **23**, 352–380 (2021).
4. Gerber, Y. *et al.* A contemporary appraisal of the heart failure epidemic in Olmsted County, Minnesota, 2000 to 2010. *JAMA Intern. Med.* **175**, 996–1004 (2015).
5. Kittleson, M. M. *et al.* 2023 ACC Expert Consensus Decision Pathway on Management of Heart Failure With Preserved Ejection Fraction: A Report of the American College of Cardiology Solution Set Oversight Committee. *J. Am. Coll. Cardiol.* **81**, 1835–1878 (2023).
6. Anker, S. D. *et al.* Patient phenotype profiling in heart failure with preserved ejection fraction to guide therapeutic decision making. A scientific statement of the Heart Failure Association, the European Heart Rhythm Association of the European Society of Cardiology, and the European Society of Hypertension. *Eur. J. Heart Fail.* **25**, 936–955 (2023).
7. Oghina, S. *et al.* The Impact of Patients With Cardiac Amyloidosis in HFpEF Trials. *JACC Heart Fail.* **9**, 169–178 (2021).

8. Redfield, M. M. Heart Failure with Preserved Ejection Fraction. *N. Engl. J. Med.* **375**, 1868–1877 (2016).

9. Lourenço, A. P. *et al.* An integrative translational approach to study heart failure with preserved ejection fraction: a position paper from the Working Group on Myocardial Function of the European Society of Cardiology. *Eur. J. Heart Fail.* **20**, 216–227 (2018).

10. Campbell, P., Rutten, F. H., Lee, M. M., Hawkins, N. M. & Petrie, M. C. Heart failure with preserved ejection fraction: everything the clinician needs to know. *Lancet Lond. Engl.* **403**, 1083–1092 (2024).

11. Pfeffer, M. A., Shah, A. M. & Borlaug, B. A. Heart Failure With Preserved Ejection Fraction In Perspective. *Circ. Res.* **124**, 1598–1617 (2019).

12. Rocca, A., Heeswijk, R. B. V., Richiardi, J., Meyer, P. & Hullin, R. The Cardiomyocyte in Heart Failure with Preserved Ejection Fraction—Victim of Its Environment? *Cells* **11**, 867 (2022).

13. Shah, S. J. *et al.* Research Priorities for Heart Failure With Preserved Ejection Fraction: National Heart, Lung, and Blood Institute Working Group Summary. *Circulation* **141**, 1001–1026 (2020).

14. Anker, S. D. *et al.* Empagliflozin in Heart Failure with a Preserved Ejection Fraction. *N. Engl. J. Med.* **385**, 1451–1461 (2021).

15. Solomon, S. D. *et al.* Dapagliflozin in Heart Failure with Mildly Reduced or Preserved Ejection Fraction. *N. Engl. J. Med.* **387**, 1089–1098 (2022).

16. Solomon, S. D. *et al.* Finerenone in Heart Failure with Mildly Reduced or Preserved Ejection Fraction. *N. Engl. J. Med.* **391**, 1475–1485 (2024).

17. Cannata, A. & McDonagh, T. A. Heart Failure with Preserved Ejection Fraction. *N. Engl. J. Med.* **392**, 173–184 (2025).

18. Senni, M. *et al.* New strategies for heart failure with preserved ejection fraction: the importance of targeted therapies for heart failure phenotypes. *Eur. Heart J.* **35**, 2797–2815 (2014).

19. Patel, R. B. & Shah, S. J. Drug Targets for Heart Failure with Preserved Ejection Fraction: A Mechanistic Approach and Review of Contemporary Clinical Trials. *Annu. Rev. Pharmacol. Toxicol.* **59**, 41–63 (2019).

20. Kosiborod, M. N. *et al.* Semaglutide in Patients with Heart Failure with Preserved Ejection Fraction and Obesity. *N. Engl. J. Med.* **389**, 1069–1084 (2023).

21. Kosiborod, M. N. *et al.* Semaglutide in Patients with Obesity-Related Heart Failure and Type 2 Diabetes. *N. Engl. J. Med.* **390**, 1394–1407 (2024).

22. Kosiborod, M. N. *et al.* Semaglutide versus placebo in patients with heart failure and mildly reduced or preserved ejection fraction: a pooled analysis of the SELECT, FLOW, STEP-HFpEF, and STEP-HFpEF DM randomised trials. *Lancet Lond. Engl.* **404**, 949–961 (2024).

23. Packer, M. *et al.* Tirzepatide for Heart Failure with Preserved Ejection Fraction and Obesity. *N. Engl. J. Med.* (2024) doi:10.1056/NEJMoa2410027.

24. Di Sopra, L., Piccini, D., Coppo, S., Stuber, M. & Yerly, J. An automated approach to fully self-gated free-running cardiac and respiratory motion-resolved 5D whole-heart MRI. *Magn. Reson. Med.* **82**, 2118–2132 (2019).

25. Deo, R. C. Machine Learning in Medicine. *Circulation* **132**, 1920–1930 (2015).

26. Pieske, B. *et al.* How to diagnose heart failure with preserved ejection fraction: the HFA-PEFF diagnostic algorithm: a consensus recommendation from the Heart Failure Association (HFA) of the European Society of Cardiology (ESC). *Eur. Heart J.* **40**, 3297–3317 (2019).

27. Svensson, J. *et al.* Few differences in cytokines between patients newly diagnosed with type 1 diabetes and their healthy siblings. *Hum. Immunol.* **73**, 1116–1126 (2012).

28. Kowalczuk, L. *et al.* Proteome and Metabolome of Subretinal Fluid in Central Serous Chorioretinopathy and Rhegmatogenous Retinal Detachment: A Pilot Case Study. *Transl. Vis. Sci. Technol.* **7**, 3 (2018).

29. Ivanisevic, J. & Thomas, A. Metabolomics as a Tool to Understand Pathophysiological Processes. *Methods Mol. Biol. Clifton NJ* **1730**, 3–28 (2018).

30. Dunn, W. B. *et al.* Procedures for large-scale metabolic profiling of serum and plasma using gas chromatography and liquid chromatography coupled to mass spectrometry. *Nat. Protoc.* **6**, 1060–1083 (2011).

31. Fan, S. *et al.* Systematic Error Removal Using Random Forest for Normalizing Large-Scale Untargeted Lipidomics Data. *Anal. Chem.* **91**, 3590–3596 (2019).

32. Magliocco, G. *et al.* Metabolomics reveals biomarkers in human urine and plasma to predict cytochrome P450 2D6 (CYP2D6) activity. *Br. J. Pharmacol.* **178**, 4708–4725 (2021).

33. Porcu, E. *et al.* Triangulating evidence from longitudinal and Mendelian randomization studies of metabolomic biomarkers for type 2 diabetes. *Sci. Rep.* **11**, 6197 (2021).

34. Wolfender, J.-L., Marti, G., Thomas, A. & Bertrand, S. Current approaches and challenges for the metabolite profiling of complex natural extracts. *J. Chromatogr. A* **1382**, 136–164 (2015).

35. Dührkop, K. *et al.* SIRIUS 4: a rapid tool for turning tandem mass spectra into metabolite structure information. *Nat. Methods* **16**, 299–302 (2019).

36. Dührkop, K. *et al.* Systematic classification of unknown metabolites using high-resolution fragmentation mass spectra. *Nat. Biotechnol.* **39**, 462–471 (2021).

37. Wingett, S. W. & Andrews, S. FastQ Screen: A tool for multi-genome mapping and quality control. *F1000Research* **7**, 1338 (2018).

38. Extramiana, F. *et al.* Computerized automated algorithm-based analyses of digitized paper ECGs in Brugada syndrome. *J. Electrocardiol.* **69S**, 61–66 (2021).

39. Kligfield, P. *et al.* Comparison of automated interval measurements by widely used algorithms in digital electrocardiographs. *Am. Heart J.* **200**, 1–10 (2018).

40. Badilini, F., Libretti, G. & Vaglio, M. Automated JTpeak analysis by BRAVO. *J. Electrocardiol.* **50**, 752–757 (2017).

41. Mitchell, C. *et al.* Guidelines for Performing a Comprehensive Transthoracic Echocardiographic Examination in Adults: Recommendations from the American Society of Echocardiography. *J. Am. Soc. Echocardiogr.* **32**, 1–64 (2019).

42. Lang, R. M. *et al.* Recommendations for Cardiac Chamber Quantification by Echocardiography in Adults: An Update from the American Society of Echocardiography and the European Association of Cardiovascular Imaging. *Eur. Heart J. – Cardiovasc. Imaging* **16**, 233–271 (2015).

43. Nagueh, S. F. *et al.* Recommendations for the Evaluation of Left Ventricular Diastolic Function by Echocardiography: An Update from the American Society of Echocardiography and the European Association of Cardiovascular Imaging. *Eur. Heart J. – Cardiovasc. Imaging* **17**, 1321–1360 (2016).

44. Smiseth, O. A. *et al.* Multimodality imaging in patients with heart failure and preserved ejection fraction: an expert consensus document of the European Association of Cardiovascular Imaging. *Eur. Heart J. - Cardiovasc. Imaging* **23**, e34–e61 (2022).

45. Coats, A. J. S. *et al.* The management of secondary mitral regurgitation in patients with heart failure: a joint position statement from the Heart Failure Association (HFA), European Association of Cardiovascular Imaging (EACVI), European Heart Rhythm Association (EHRA), and European Association of Percutaneous Cardiovascular Interventions (EAPCI) of the ESC. *Eur. Heart J.* **42**, 1254–1269 (2021).

46. Baumgartner, H. *et al.* Recommendations on the echocardiographic assessment of aortic valve stenosis: a focused update from the European Association of Cardiovascular Imaging and the American Society of Echocardiography. *Eur. Heart J. Cardiovasc. Imaging* **18**, 254–275 (2017).

47. Lancellotti, P. *et al.* Multi-modality imaging assessment of native valvular regurgitation: an EACVI and ESC council of valvular heart disease position paper. *Eur. Heart J. Cardiovasc. Imaging* **23**, e171–e232 (2022).

48. Vasu, S. *et al.* Regadenoson and adenosine are equivalent vasodilators and are superior than dipyridamole- a study of first pass quantitative perfusion cardiovascular magnetic resonance. *J. Cardiovasc. Magn. Reson. Off. J. Soc. Cardiovasc. Magn. Reson.* **15**, 85 (2013).

49. Kato, S. *et al.* Prognostic significance of quantitative assessment of focal myocardial fibrosis in patients with heart failure with preserved ejection fraction. *Int. J. Cardiol.* **191**, 314–319 (2015).

50. Kellman, P. *et al.* Bright-blood and dark-blood phase sensitive inversion recovery late gadolinium enhancement and T1 and T2 maps in a single free-breathing scan: an all-in-one approach. *J. Cardiovasc. Magn. Reson.* **23**, 126 (2021).

51. Christensen, R. H., Lundgren, T., Stenvinkel, P. & Brismar, T. B. Renal volumetry with magnetic resonance imaging. *Acta Radiol. Open* **6**, 2058460117731120 (2017).

52. Milani, B. *et al.* Reduction of cortical oxygenation in chronic kidney disease: evidence obtained with a new analysis method of blood oxygenation level-dependent magnetic resonance imaging. *Nephrol. Dial. Transplant.* **32**, 2097–2105 (2017).

53. Calarnou, P. *et al.* Navigator acceptance window width does not affect accuracy and precision in free-breathing 2D cardiac MR fingerprinting of the myocardium at 3T. in *Proc Int Soc Magn Reson Med, Toronto* 3999 (Toronto, 2023).

54. Vincenti, G. *et al.* Compressed Sensing Single–Breath-Hold CMR for Fast Quantification of LV Function, Volumes, and Mass. *JACC Cardiovasc. Imaging* **7**, 882–892 (2014).

55. Xue, H., Brown, L. A. E., Nielles-Vallespin, S., Plein, S. & Kellman, P. Automatic in-line quantitative myocardial perfusion mapping: Processing algorithm and implementation. *Magn. Reson. Med.* **83**, 712–730 (2020).

56. Ma, L. E. *et al.* Aortic 4D flow MRI in 2 minutes using compressed sensing, respiratory controlled adaptive k-space reordering, and inline reconstruction. *Magn. Reson. Med.* **81**, 3675–3690 (2019).

57. Piccini, D., Littmann, A., Nielles-Vallespin, S. & Zenge, M. O. Spiral phyllotaxis: the natural way to construct a 3D radial trajectory in MRI. *Magn Reson Med* **66**, 1049–56 (2011).

58. Montón Quesada, I. *et al.* Self-gated free-running 5D whole-heart MRI using blind source separation for automated cardiac motion extraction. *Magn Reson Med Press* (2024) doi:10.1002/mrm.30322.

59. Ogier, A. C. *et al.* Free-running 5D whole-heart MRI for isotropic cardiac function measurements at 3T without contrast agents. *Magn Reson Med* **In Press**, (2025).

60. Feng, L. *et al.* 5D whole-heart sparse MRI. *Magn. Reson. Med.* **79**, 826–838 (2018).

61. Reddy, Y. N. V., Carter, R. E., Obokata, M., Redfield, M. M. & Borlaug, B. A. A Simple, Evidence-Based Approach to Help Guide Diagnosis of Heart Failure With Preserved Ejection Fraction. *Circulation* **138**, 861–870 (2018).

62. Aslam, I. *et al.* Validation of automatically measured T1 map cortico-medullary difference (ΔT1) for eGFR and fibrosis assessment in allograft kidneys. *PLOS ONE* **18**, e0277277 (2023).

63. Kowallick, J. T. *et al.* Quantification of atrial dynamics using cardiovascular magnetic resonance: inter-study reproducibility. *J. Cardiovasc. Magn. Reson.* **17**, 36 (2015).

64. Dellegrottaglie, S. *et al.* Pulmonary Hypertension: Accuracy of Detection with Left Ventricular Septal-to–Free Wall Curvature Ratio Measured at Cardiac MR. *Radiology* **243**, 63–69 (2007).

65. Cerqueira, M. D. *et al.* Standardized myocardial segmentation and nomenclature for tomographic imaging of the heart. *Circulation* **105**, 539–42 (2002).

66. Vargas-Barron, J. *et al.* Prognostic Implications of Right Atrial Ischemic Dysfunction in Patients with Biventricular Inferior Infarction: Transesophageal Echocardiographic Analysis. *Echocardiography* **18**, 105–112 (2001).

67. Kellman, P. *et al.* Myocardial perfusion cardiovascular magnetic resonance: optimized dual sequence and reconstruction for quantification. *J. Cardiovasc. Magn. Reson.* **19**, 43 (2016).

68. Georgantas, C., Banus, J., Hullin, R. & Richiardi, J. Systematic Estimation of Treatment Effect on Hospitalization Risk as a Drug Repurposing Screening Method. in *Biocomputing 2024* 232–246 (WORLD SCIENTIFIC, Kohala Coast, Hawaii, USA, 2023). doi:10.1142/9789811286421_0019.

69. Truong, V. Q. *et al.* Quality Control Procedures for Genome-Wide Association Studies. *Curr. Protoc.* **2**, e603 (2022).

70. Privé, F., Aschard, H., Ziyatdinov, A. & Blum, M. G. B. Efficient analysis of large-scale genome-wide data with two R packages: bigstatsr and bigsnpr. *Bioinformatics* **34**, 2781–2787 (2018).

71. Graubert, A., Aguet, F., Ravi, A., Ardlie, K. G. & Getz, G. RNA-SeQC 2: efficient RNA-seq quality control and quantification for large cohorts. *Bioinformatics* **37**, 3048–3050 (2021).

72. Patro, R., Duggal, G., Love, M. I., Irizarry, R. A. & Kingsford, C. Salmon provides fast and bias-aware quantification of transcript expression. *Nat. Methods* **14**, 417–419 (2017).

73. Dobin, A. *et al.* STAR: ultrafast universal RNA-seq aligner. *Bioinformatics* **29**, 15–21 (2013).

74. Putri, G. H., Anders, S., Pyl, P. T., Pimanda, J. E. & Zanini, F. Analysing high-throughput sequencing data in Python with HTSeq 2.0. *Bioinformatics* **38**, 2943–2945 (2022).

75. Georgantas, C., Kutalik, Z. & Richiardi, J. Deep Learning for Polygenic Risk Prediction. Preprint at https://doi.org/10.1101/2024.04.19.24306079 (2024).

76. Zitnik, M. *et al.* Machine learning for integrating data in biology and medicine: Principles, practice, and opportunities. *Inf. Fusion* **50**, 71–91 (2019).

77. Prasser, F., Kohlmayer, F., Lautenschläger, R. & Kuhn, K. A. ARX--A Comprehensive Tool for Anonymizing Biomedical Data. *AMIA Annu. Symp. Proc. AMIA Symp.* **2014**, 984–993 (2014).

78. Ziegenhain, C. & Sandberg, R. BAMboozle removes genetic variation from human sequence data for open data sharing. *Nat. Commun.* **12**, 6216 (2021).

79. Gürsoy, G. *et al.* Data Sanitization to Reduce Private Information Leakage from Functional Genomics. *Cell* **183**, 905-917.e16 (2020).

80. Holzinger, A., Haibe-Kains, B. & Jurisica, I. Why imaging data alone is not enough: AI-based integration of imaging, omics, and clinical data. *Eur. J. Nucl. Med. Mol. Imaging* **46**, 2722–2730 (2019).

81. McGillivray, P. *et al.* Network Analysis as a Grand Unifier in Biomedical Data Science. *Annu. Rev. Biomed. Data Sci.* **1**, 153–180 (2018).

82. Cavalli, F. M. G. *et al.* Intertumoral Heterogeneity within Medulloblastoma Subgroups. *Cancer Cell* **31**, 737-754.e6 (2017).

Supplemental Material

Supplementary Table 1. Clinical chemistry obtained from the blood samples.

Blood parameter	Unit
Sodium	mmol/l
Potassium	mmol/l
Chloride	mmol/l
Total calcium	mmol/l
Corrected calcium	mmol/l
Total magnesium	mmol/l
Phosphate	mmol/l
Osmolality	mmol/Kg H_2O
Calculated osmolality	mmol/Kg H_2O
Osmolar gap	mmol/Kg H_2O
Venous glucose	mmol/l
Creatinine (Jaffé)	µmol/l
Urea	mmol/l
Total cholesterol	mmol/l
HDL	mmol/l
Non-HDL	mmol/l
Triglycerides	mmol/l
Calculated LDL-cholesterol	mmol/l
Urate	µmol/l
Total bilirubin	µmol/l
Direct bilirubin	µmol/l
Iron	µmol/l
Albumin	g/l
CRP	mg/l
Transferrin	µmol/l
Transferrin saturation coef.	
Ferritin	µg/l
Hs-troponin T	ng/l
CK	U/l
CK-MB	U/l
LDH	U/l
AST (GOT)	U/l
ALT(GPT)	U/l
Ɣ-GT	U/l

Pancreatic amylase	U/l
Lipase	U/l
Alkaline phosphatase	U/l
Measured bicarbonate	mmol/l
Anion gap	mmol/l
eGFR (CKD-EPI creatinine)	ml/min/1.73m^2
NT-proBNP	ng/l
Haptoglobin	g/l
Procalcitonin	µg/l
Serum proteins	g/l
TSH	mUI/l
Total T4	nmol/l
Free T4	pmol/l
Total T3	nmol/l
Free T3	pmol/l
Reverse T3	nmol/l
Prealbumin	g/l
Free carnitine	µmol/l
Total carnitine	µmol/l
Acyl-carnitine	µmol/l
Acyl-Carnitine/Free Carnitine	mol/mol
Acylcarnitine's profil	µmol/l
Carnitine (C0)	µmol/l
Acetyl carnitine (C2)	µmol/l
Propionyl carnitine (C3)	µmol/l
Malonyl carnitine (C3DC)	µmol/l
Methyl malonyl carnitine (C32MDC)	µmol/l
Butyryl carnitine (C4)	µmol/l
Hydroxy butyryl carnitine (C4OH)	µmol/l
Succinyl carnitine (C4DC)	µmol/l
3-hydroxyisovalerylcarnitine/2-methyl-3-	µmol/l
Tiglylcarnitine/3-methylcrotonylcarnitine (C5:1)	µmol/l
Isovalerylcarnitine/2-methylbutyrylcarnitine (C5)	µmol/l
Glutaryl carnitine (C5DC)	µmol/l
Hexanoyl carnitine (C6)	µmol/l

3-hydroxyhexanoycarnitine (C6OH)	µmol/l
Adipyl carnitine/3-methylglutarylcarnitine (C6DC)	µmol/l
Heptanoyl carnitine (C7)	µmol/l
Octenyl carnitine (C8:1)	µmol/l
Octanol carnitine (C8)	µmol/l
3-hydroxyoctanylcarntine (C8OH)	µmol/l
Suberoylcarnitne (C8DC)	µmol/l
Decadienoylcarnitine (C10:2)	µmol/l
Decenylcarnitine (C10:1)	µmol/l
Decanoyl carnitine (C10)	µmol/l
3-hydroxydecanoylcarnitine (C10OH)	µmol/l
Dodecenoylcarnitine (C12:1)	µmol/l
Dodecanoyl carnitine (C12)	µmol/l
3-hydroxydodecanoylcarnitine (C12OH)	µmol/l
Tetradecadienoylcarnitine (C14:2)	µmol/l
Tetradecenoyl carnitine (C14:1)	µmol/l
Tetradecanoyl carnitine (C14)	µmol/l
3-hydroxytetradecenoyalcarnitine (C14:1OH)	µmol/l
3-hydroxytetradecanoylcarnitine (C14OH)	µmol/l
Palmitoleylcarnitine (C16:1)	µmol/l
Palmitoyl carnitine (C16)	µmol/l
3-hydroxypalmitoleylcarnitine (C16:1OH)	µmol/l
3-hydroxypalmitoylcarnitine (C16OH)	µmol/l
Linoleylcarnitine (C18:2)	µmol/l
Oleyl carnitine (C18:1)	µmol/l
Stearoyl carnitine (C18)	µmol/l
3-hydroxylinoleylcarnitine (C18:2OH)	µmol/l
3-hydroxyoleylcarnitine (C18:1OH)	µmol/l
3-hydroxystearoylcarnitine (C18OH)	µmol/l
C3/C4 ratio	
C4/C2 ratio	
C5/C3 ratio	
C5DC/C3 ratio	
C8/C10 ratio	
C8/C10:1 ratio	

C14:1/C18:1 ratio	
C16OH/C16 ratio	
C0/(C16+C18) ratio	
C2/(C16+C18) ratio	
C14:1/C12:1 ratio	
(C16+C18:1)/C2 ratio	
Leukocytes	G/l
Erythrocytes	T/l
Haemoglobin	g/l
Haematocrit	%
MCV	fl
MCH	pg
MCHC	g/l
RDW	%
Platelets	G/l
Mean platelet volume	fl
Platelet distribution width	fl
Erythroblasts (automated)	/100 leuko.
Reticulocytes	°/oo
Absolute reticulocytes	G/l
Immature reticulocyte fraction	%
Immature reticulocytes	%
Haemoglobin concentration in reticulocytes	pg

1

Supplementary Table 2. 2D echocardiographic acquisition details, including the measurements from each imaging window.

Imaging window	Linear measurements	M-Mode/Areas/Volumes	Color Doppler	Spectral Doppler
Parasternal long axis	Septal thickness (mm) Posterior wall thickness (mm) LV diastolic diameter (mm) LV systolic diameter (mm) Left atrial diameter (mm) LVOT diameter (mm) Aortic root diameter (mm) Sino-tubular junction (mm) Ascending aorta (mm)		Vena contracta (if AR or MR present)	

	RVOT diameter (mm)			
Parasternal RV inflow view			Vena contracta (if TR present) PISA radius (if TR present)	Tricuspid regurgitation (CwD)
Parasternal short axis (aortic)	Main pulmonary artery (mm) RVOT diameter (mm)	Aortic valve planimetry	Vena contracta (if TR present) PISA radius (if TR present)	Tricuspid regurgitation (CwD) Pulmonary valve flow (CwD) RVOT flow (PwD)
Parasternal short axis (mitral)		Mitral valve planimetry	MR ellipticity	
Parasternal SAX (papillary)				
Parasternal short axis (apex)				
Apical 4-chambers		Left atrial volume Diastolic LV volume Systolic LV volume	Vena contracta (if MR present) PISA radius (if MR present)	Mitral inflow leaflet tip (PwD) Mitral inflow annulus (PwD) Pulmonary vein flow (PwD)

				Mitral inflow (CwD) Mitral regurgitation (CwD) Septal mitral annulus (TD) Lateral mitral annulus (TD)
Apical 2-chambers	Descending aorta diam (mm)	Left atrial volume Diastolic LV volume Systolic LV volume		
Apical 3-chambers			Vena contracta (if MR present) PISA radius (if MR present)	
Apical 5-chambers			Vena contracta (if AR present) PISA radius (if AR present)	Aortic outflow (CwD) Aortic regurgitation flow (CwD) LVOT flow (PwD)

RV-modified 4-chambers view	RV basal diameter (mm) RV mid diameter (mm) RV length (mm)	Right atrial volume Right atrial area RV diastolic area RV systolic area TAPSE	Vena contracta (if TR present) PISA radius (if TR present)	Tricuspid inflow (PwD) Tricuspid inflow (CwD) Tricuspid regurgitation (CwD) Tricuspid annulus (TD)
Sub-costal long axis				Tricuspid regurgitation (CwD)
Sub-costal short axis	Same as parasternal SAX			
Vena cava long axis view	Diameter exspiration (mm) Diameter inspiration (mm) Diameter snif (mm)	M-Mode IVC diameter		Hepatic vein flow (PwD)
Abdominal aorta (SAX/LAX)	Diameter (mm)			Flow in AR present (PwD)
Supra-sternal	Aortic arch diameter (mm)			Aortic arch flow (CwD)

				Aortic arch flow (PwD) if AR present
Pedoff probe (suprasternal, apical/right parasternal				Aortic outflow (CwD) if AS present

Supplementary Table 3. Measured and calculated MRI Parameters for each pulse sequence. Units are mentioned in parentheses when relevant, as is the subdivision. The subdivisions of the CMR parameters are: WH whole heart, 3P three planes, AHA16/AHA17 the 16 or 17 segments defined by the American Heart Association (i.e. excluding the apex or not), and S-D means quantified for both systole and diastole.

Sequence	**Images**	**Measurements**
HASTE	Stack of 2D T_2-weighted kidney images	Kidney volume (mm^3), cortex volume, medulla volume, cortex diameter
BOLD	Single 2D R2*map	Cortex T_2* (ms), Medulla T_2* (ms)
Kidney PARMA	Single 2D T_1&T_2 map	Cortex T_1 (ms), Medulla T_1 (ms), Cortex T_2 (ms), Medulla T_2 (ms)
Heart PARMA	4 2D T_1&T_2 maps, before and after GBCA injection	Myocardial T_1 (ms, WH/3P/AHA17), Myocardial T_2 (ms, WH/3P/AHA17), Myocardial ECV (ms, WH/3P/AHA17), Blood T_1 (ms)
2D cine	Stack of 10-12 dynamic 2D heart images	Myocardial volume (mL, AHA17), LV volume (mL, S-D), RV volume (mL, S-D), LV EF (%), RV EF (%), LV stroke volume (mL), RV stroke volume (mL)

qPerf	3 dynamic GBCA perfusion images and 3 quantitative perfusion maps, under pharmacological stress and at rest	Stress perfusion (mL/min/g, WH/3P/AHA16), Rest perfusion (mL/min/g, WH/3P/AHA16), Myocardial perfusion reserve (-,WH/3P/AHA16)
5D FRF	5D (3D+respiratory&cardiac cycles) T_1-weighted whole-heart image	Myocardial volume (mL, AHA17), LV volume (mL, S-D), RV volume (mL, S-D), LV EF (%), RV EF (%), LV stroke volume (mL), RV stroke volume (mL)
4D flow	4D (3D spatial + cardiac cycle) flow in 3 directions	Asc. aorta peak flow (mL/s), Asc. aorta net flow volume (mL), Desc. aorta peak flow (mL/s), Desc. aorta net flow volume (mL), Main pulmonary artery peak velocity (cm/s), Main pulmonary artery net flow volume (mL), Mitral valve inflow peak velocity (cm/s), Mitral valve inflow net flow volume (mL), Mitral regurgitant fraction (%), Tricuspid valve inflow peak velocity (cm/s), Tricuspid valve inflow net flow volume (mL), Tricuspid

		regurgitant fraction (%), Left ventricle outflow net flow volume (mL), Right ventricle outflow net flow volume (mL)

Supplementary Table 4. Collected clinical parameters.

Demographic parameters	
Year of birth	
Sex	
Ethnicity	
Anthropometric parameters	
Weight	Kg
Height	Cm
BMI	Kg/m^2
Consumption habits	
Smoking	Yes/No
If yes	
Years of smoking	Year
Number of cigarettes	Number/Day
Alcohol	Yes/No
If yes	
Years of alcohol use	Year
Number of standard drinks per occasion	
Drug	Yes/No
Medical history	
Cardiovascular	
Coronary disease	Yes/No
Myocardial infarction	Yes/No
Family history of coronary artery disease	Yes/No
Previous hospitalization for HF	Yes/No
Aortic stenosis	Yes/No
Aortic regurgitation	Yes/No
Mitral stenosis	Yes/No
Mitral regurgitation	Yes/No
Tricuspid regurgitation	Yes/No
Equipped with pacemaker or cardiac implant	Yes/No
Dyslipidaemia	Yes/No
Atrial fibrillation	Yes/No
Peripheral artery disease	Yes/No

Other	
Medication history	
Medication	Yes/No
If yes	
Name(s) of the medication(s)	
Frequency	
Dosage	
Indication	
Women only	
Ever used hormonal contraception	Yes/No
If yes	
Name of the contraception	
Dosage	
Route of administration	
Menopause	Yes/No
If yes	
Ever used hormone replacement therapy (HRT)	Yes/No
COMORBIDITIES	
Obesity	Yes/No
Diabetes mellitus	Yes/No
Hypertension	Yes/No
Renal dysfunction	Yes/No
Anemia	Yes/No
Iron deficiency	Yes/No
Sleep disorder	Yes/No
Chronic obstructive pulmonary disease (COPD)	Yes/No
VITAL SIGNS	
Temperature	℃
Heart rate	bpm
Blood pressure (TAS/DAS)	mmHg
Respiratory rate	bpm